Research Square

Preprints are preliminary reports that have not undergone peer review.
They should not be considered conclusive, used to inform clinical practice,
or referenced by the media as validated information.

Design and field response analysis of double-sided staged hydraulic fracturing in gob-side entry under multi-layer hard roof condition

Tianwei Lan
College of Mining, Liaoning Technical University
Yuhang Wu
131041423850163.com

College of Mining, Liaoning Technical University
Yonghao Liu
College of Mining, Liaoning Technical University
Zhijia Zhang
College of Mining, Liaoning Technical University
Tianqi Wei
College of Mining, Liaoning Technical University
Bole Li
College of Mining, Liaoning Technical University
Lutong Niu
College of Mining, Liaoning Technical University

Article

Keywords:

Posted Date: November 5th, 2026

DOI: https://doi.org/10.21203/rs.3.rs-11377381/v1

License: This work is licensed under a Creative Commons Attribution 4.0 International License.
Read Full License

Additional Declarations: No competing interests reported.

Design and field response analysis of double-sided staged hydraulic fracturing in gob-side entry under multi-layer hard roof condition

Tianwei Lan[1,2] *, Yuhang Wu[1], Yonghao Liu[1],Zhijia Zhang[1],Tianqi Wei[1],Bole Li[1],Lutong Niu[1]

1 College of Mining, Liaoning Technical University, Fuxin China；

2. Ordos Institute of Liaoning Technical University, Ordos China；

* Corresponding author

E-mail: 13104142385@163.com (TW.L)

Abstract

Aiming at the problem of deformation and fracturing treatment location determination of gob-side entry under the condition of multi-layer hard rock roof, based on the engineering data of I030902 working face in Limin Coal Mine, the combined beam load screening and numerical simulation were used to determine the fracturing horizon and its lateral loading position, and the staged hydraulic fracturing scheme of bilateral long and short holes was analyzed. Combined with surrounding rock deformation, support load, hole wall peep and microseismic records, the field response and effect were evaluated. The results show that Y2, Y8 and Y13 can be used as the design focus layers. The stress concentration positions of Y2 and Y8 are close to the gob-side entry, and the peak value of Y13 is biased to the old goaf side. The approximate maximum deformation of the roof and floor direction, coal pillar side and solid coal side of the unfractured section and the fractured section is about 225 mm, 180 mm, 125 mm and about 22 mm, 18 mm, 12 mm, respectively. The average working resistance of the two sections of the support is 9725 kN and 8943 kN respectively, and the fracturing section is about 8 % lower ; the microseismic records of the fracturing section are dominated by $10^1 \sim 10^2$ J events, and no events of 10^4 J and above are shown. The field response is generally consistent with the design goals of reducing deformation and reducing load, but the information of mining stage, monitoring window and supporting conditions is incomplete, and the existing data cannot separate the independent contribution of fracturing.

1. Introduction

Under multiple hard roof strata, the roof may not cave completely after extraction, leaving a hanging roof and causing pronounced ground pressure manifestations[1]. For a gob-side roadway adjacent to an old goaf and protected by a narrow coal pillar, surrounding rock stability is governed jointly by the overburden structure, coal pillar load bearing, and mining disturbance[2,3]. Surrounding rock control can involve both support reinforcement and pressure relief, with the applicability of each measure considered[4,5]. When several hard strata occur above the coal seam, their failure and load transfer at different elevations complicate roof treatment. The strata requiring control should therefore be identified by considering the overburden structure and both near-field and far-field effects[6].

Identifying the target strata is fundamental to roof weakening design. Xu et al.[7] proposed identifying the principal controlling strata from the complete overburden sequence and interactions among strata. Through physical and numerical investigations, Xia et al.[8] examined target stratum selection for surface hydraulic fracturing of multiple hard roofs, demonstrating that treating different strata produces different stress and failure responses. Zhang et al.[9] investigated the relationship between presplitting-induced weakening of hard overburden and fracture zone development. Gao et al.[10] analyzed changes in block size and structural evolution through full-stratum presplitting blasting of a high-level stratum. These studies indicate that treatment stratum selection should account for geological occurrence and each stratum's role in overburden movement.

Numerical simulation provides a means of analyzing fracturing parameters and roof responses. Wang et al.[11] investigated the effects of fracture spacing, fracture height, and treatment stratum on

the collapse of thick, hard roofs. Wu et al.[12] used a fluid-solid coupled discrete element method to analyze surrounding rock responses under coal pillar and thick, hard roof conditions. Li et al.[13] used a phase-field model to investigate the relationship between fracture networks and stress evolution around roadways. Hua et al.[14] further examined the effects of borehole angle and placement stratum on fracture propagation in composite hard roofs. These studies provide a basis for parameter checking and show that design parameters should be related to lithology and stress conditions.

For underground engineering applications, Kang et al.[15] developed directional borehole hydraulic fracturing technology covering stratum selection, borehole design, fracturing operations, and monitoring-based evaluation. Niu[16] and Hu et al.[17] investigated roof control by staged fracturing and the associated stress and fracture evolution, respectively. For gob-side roadways, Zhang et al.[18] combined hydraulic slotting and fracturing to analyze how roof structure modification affects surrounding rock loading. Tan et al.[19] combined target stratum analysis with multidimensional staged fracturing using long directional boreholes and conventional shallow boreholes, providing an engineering reference for treating different locations.

Fracturing schemes also require adjustment to field conditions and evaluation through multiple observations. Wang et al.[20] adjusted a treatment scheme to the geological occurrence of multiple thick, hard roof strata. Lei et al.[21] investigated the effects of injection rate on fracture dimensions and conducted ground pressure and microseismic monitoring. Zhuang et al.[22] and Ma et al.[23] combined numerical analysis with field data to evaluate fracturing effects through mining-induced stress, overburden movement, and microseismic responses. In a study of surface fracturing of multiple thick, hard roofs, Wu et al.[24] compared the proportion of high-energy events and their frequency per unit face advance, providing a reference method for evaluating field responses.

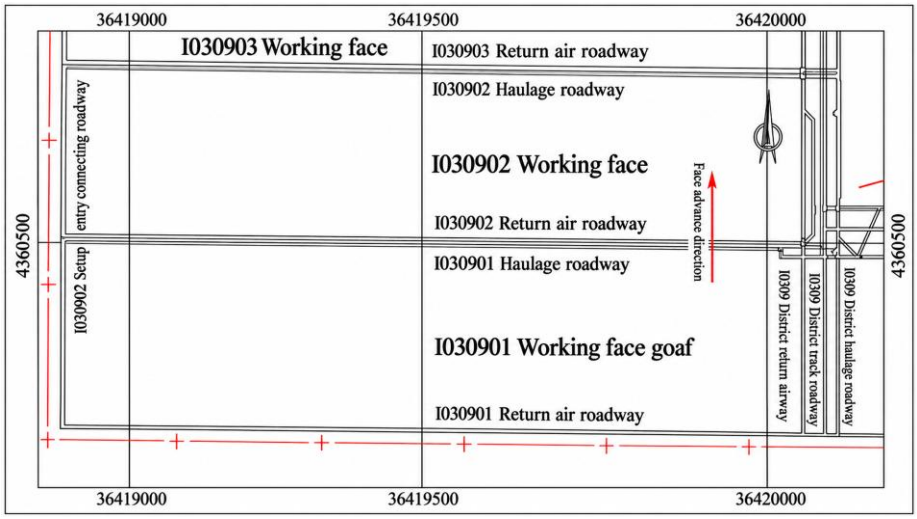
For gob-side roadways beneath multiple hard roof strata, the relationship between target strata and lateral loading positions must be established, and the treatment requirements at different elevations and lateral positions must be incorporated into the arrangement of long and short boreholes. Field evaluation should also distinguish design objectives from actual observations and account for differences in mining stage and monitoring window between comparison sections. This study focuses on the gob-side return airway of the I030902 working face at Limin Coal Mine. Target strata are screened using the overburden sequence, physical and mechanical properties, and a composite-beam load criterion. Numerical simulation is then used to analyze lateral loading positions in each stratum. On this basis, long and short boreholes are arranged on both sides of the roadway for staged hydraulic fracturing. Field responses in the test section are evaluated using surrounding rock deformation, hydraulic support working resistance, borehole wall inspection, and microseismic records.

2. Engineering conditions

2.1 Working face and gob-side roadway layout

The I030902 working face lies in the southwestern part of the Limin Coal Mine field and extracts the No. 9 coal seam at a depth of 328-486 m, averaging 407 m. The setup entry is 280 m long. The coal seam dips at 3-7 degrees, averaging 5 degrees, and is 3.18-4.32 m thick, averaging 3.75 m. Mining follows the coal seam floor without leaving bottom coal. The mined-out I030901 working face lies on one side of I030902, while the unmined I030903 working face lies on the other. The I030902 return airway is developed along the I030901 goaf with a 5 m coal pillar. Figure 1

109 shows the working face and adjacent mining spaces.



110

111 **Figure 1.** Layout of the working face and adjacent mining spaces.

2.2 Occurrence of roof strata

At the I030902 working face of Limin Coal Mine, the immediate roof comprises 5.37 m of sandy mudstone, and the main roof comprises 4.52 m of coarse-grained sandstone. Several sandstone and siltstone strata occur in the overburden, some with relatively large thicknesses and high strengths. The immediate floor is 0.84 m of mudstone, and the main floor is 2.03 m of sandy mudstone. Figure 2 shows the lithologic column of borehole BK8 at Limin Coal Mine.

Rock type	Lithologic column	Depth (m)	Thickness (m)	Lithologic description
1. Coarse-grained sandstone		264.83	6.11	Light gray, thick-bedded; predominantly feldspar and quartz; reddish-brown argillaceous cement; poorly sorted, subangular grains.
2. Siltstone		270.94	6.95	Purplish brown, massive, irregular fracture; minor platy mica.
3. Mudstone		277.89	1.89	Gray-green, thick-bedded, stepped fracture; readily weathered.
4. Coarse-grained sandstone		279.78	20.30	Predominantly gray-green; minor purplish-red spots in the upper part; joints developed; thick-bedded; lower core fragmented.
5. Mudstone		300.08	5.44	Purplish brown, thin-bedded, fine-textured.
6. Sandy mudstone		305.52	4.43	Gray-green with purple mottling, medium-thick beds; locally lenticular bedding; grades downward into fine-grained sandstone.
7. Mudstone		309.95	1.38	Gray-green, locally stained reddish brown; massive; minor sandy material; fractures developed.
8. Siltstone		311.33	2.19	Gray-green with purple mottling, thick-bedded; core fragmented; minor biotite; occasional slickensides.
9. Coarse-grained sandstone		313.52	2.33	Light gray, thick-bedded; predominantly quartz and feldspar; argillaceous cement; poorly sorted; cross bedding and horizontal bedding in lower part.
10. Sandy mudstone		315.85	4.10	Dark gray, thin-bedded, stepped fracture.
11. Coarse-grained sandstone		319.95	10.19	Light gray, medium-thick beds; mainly quartz and feldspar; argillaceous cement; high matrix content; poor mineral sorting; minor argillaceous inclusions.
12. Mudstone		330.14	1.17	Dark gray, massive, uniform texture; thin siltstone interbeds in lower part; readily weathered.
13. Coal		331.31	0.35	Black, semi-dull coal; banded structure; bedded.
14. Siltstone		331.66	0.35	Light gray, thin-bedded; black muddy streaks; lenticular bedding poorly developed.
15. Mudstone		332.01	2.92	Light gray, medium-thick beds; indistinct bedding; stepped fracture.
16. Siltstone		334.93	6.49	Light gray, thin-bedded; lenticular bedding developed; thin fine-grained sandstone interbeds; wavy bedding present.
17. Coal seam 8		341.42	0.26	Black, semi-dull coal.
18. Siltstone		341.68	2.25	Dark gray, thick-bedded; abundant calcite.
19. Sandy mudstone		343.93	4.64	Light gray, locally yellowish brown; thin-bedded; black muddy streaks; lenticular bedding developed; stepped fracture.
20. Fine-grained sandstone		348.57	3.36	Light gray, medium-thick beds; wavy bedding developed; argillaceous cement; minor biotite minerals.
21. Mudstone		350.42	1.85	Dark gray, medium-thick beds; fracture fragmented and rough.
22. Coarse-grained sandstone		354.94	4.52	Light gray, thick-bedded; predominantly quartz and feldspar; argillaceous cement; poor sorting; minor biotite in lower part.
23. Sandy mudstone		357.29	5.37	Dark gray, thin-bedded; nearly horizontal bedding; abundant calcite; flat fracture.
24. Coal seam 9-1		366.34	3.12	Black, semi-dull coal; finely banded structure; bedded; endogenous fissures developed; bituminous luster; local bright-coal bands and coal streaks; uneven fracture.
25. Mudstone		366.81	0.47	Dark gray, massive; minor coal streaks; easily stains hands.
26. Coal seam 9-2		367.54	0.73	Black, semi-dull coal; finely banded structure; bedded; endogenous fissures developed; bituminous luster; local bright-coal bands and coal streaks; uneven fracture.
27. Mudstone		368.38	0.84	Dark gray, massive; minor coal streaks; easily stains hands.
28. Sandy mudstone		370.41	2.03	Dark gray, massive; abundant calcite; black muddy streaks.

Figure 2. Lithologic column of borehole BK8 at Limin Coal Mine.

2.3 Field maintenance problems and study object

During extraction of the I030902 working face, incomplete local roof caving occurred. Deformation of the coal pillar rib, floor cracking, and floor heave developed in the gob-side return airway, affecting roadway transport. Surrounding rock deformation increased progressively with mining disturbance, making roadway stability during extraction an engineering problem requiring attention.

Extraction of I030901 had already formed a goaf, while I030902 was subjected to extraction-induced disturbance. Stability analysis therefore needs to consider both the lateral overburden structure beside the goaf and the advance of the current working face. Field deformation alone is insufficient to identify the specific contribution of each roof stratum; further analysis of the complete overburden sequence and load-bearing characteristics is required.

3. Basis for target stratum selection and borehole design

3.1 Identification of target strata

Empirical calculations indicate that the maximum caving zone height above I030902 is approximately 13.2 m and the maximum water-conducting fracture zone height is approximately 51.6 m. Surface borehole observations at the adjacent I030905 working face indicated a fracture zone height of approximately 55.6 m. Its coal seam and roof conditions are similar to those of I030902, making it a useful analog. This study focuses on the near-seam overburden above the coal seam roof and below the estimated upper boundary of the fracture zone.

Overburden analysis should consider geological occurrence and interactions among strata to identify those that exert principal control over mining-induced movement. The position and failure conditions of key strata also affect overburden fracture distribution and development height[7,25,26]. Assuming uniformly distributed loading and compatible deformation of a composite beam, a composite-beam load relationship is used to screen candidate load-bearing strata. Taking stratum k as the current starting stratum and progressively including the overlying strata, its assigned load is:

$$q_{k,n} = \frac{E_k h_k^3}{\sum_{i=k}^{n} E_i h_i^3} \sum_{i=k}^{n} \gamma_i h_i \tag{1}$$

In the formula: k is the number of the current starting stratum;n is the number of the highest stratum included in the calculation; E_i denotes the elastic modulus of each stratum; h_i denotes the thickness of each stratum, γ_i in m; denotes the unit weight of each stratum, in kN/m³; $q_{k,n}$ is the load assigned to stratum k within the composite interval from stratum k to stratum n, in kPa.

When including stratum n+1 results in $q_{k,n+1} < q_{k,n}$, the newly included stratum is identified as a candidate load-bearing stratum, and the calculation is restarted from that stratum.

The calculation initially starts from stratum Y1 and is restarted whenever a new candidate load-bearing stratum is identified. Based on the composite-beam load criterion, Y2, Y8, and Y13 are selected as the intended fracturing strata. Their occurrence and mechanical properties are listed in Table 1, and the load screening results are given in Table 2.

Stratum	Lithology	Thickness /m	Base elevation /m	Top elevation /m	Elastic modulus /GPa	Tensile strength /MPa
Y2	Coarse-grained sandstone	4.52	5.37	9.89	22.56	7.71
Y8	Siltstone	6.49	22.25	28.74	23.42	4.78
Y13	Coarse-grained sandstone	10.19	33.53	43.72	20.47	6.89

Table 1. Occurrence and mechanical properties of the intended fracturing strata.

Newly included stratum	Starting stratum	Load before inclusion /kPa	Load after inclusion /kPa
Y2	Y1	132.1	101.69
Y8	Y2	218.69	116.46
Y13	Y8	271.04	120.83

Table 2. Load screening results for candidate load-bearing strata.

These load calculations screen candidate load-bearing strata and do not directly describe the actual failure state of each stratum. Presplitting and weakening different target strata may produce different overburden movement and fracture development responses. Numerical simulation is therefore used to compare the lateral loading positions of Y2, Y8, and Y13.

3.2 Numerical simulation method

A numerical model is established using the geological and mining conditions of the fully mechanized I030901 and I030902 working faces at Limin Coal Mine. It incorporates the extraction sequence and occurrence of hard strata. The model measures 704 m × 600 m × 113 m, as shown in Figure 3.

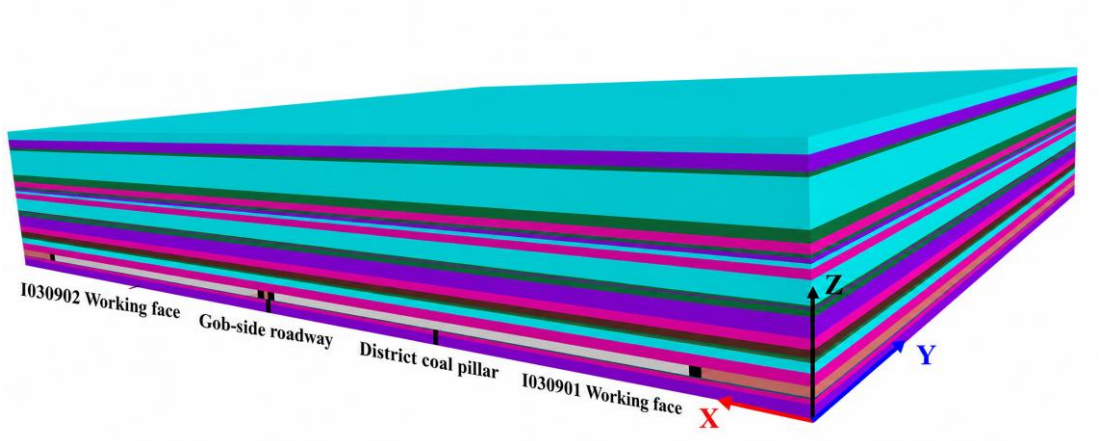


Figure 3. Numerical model.

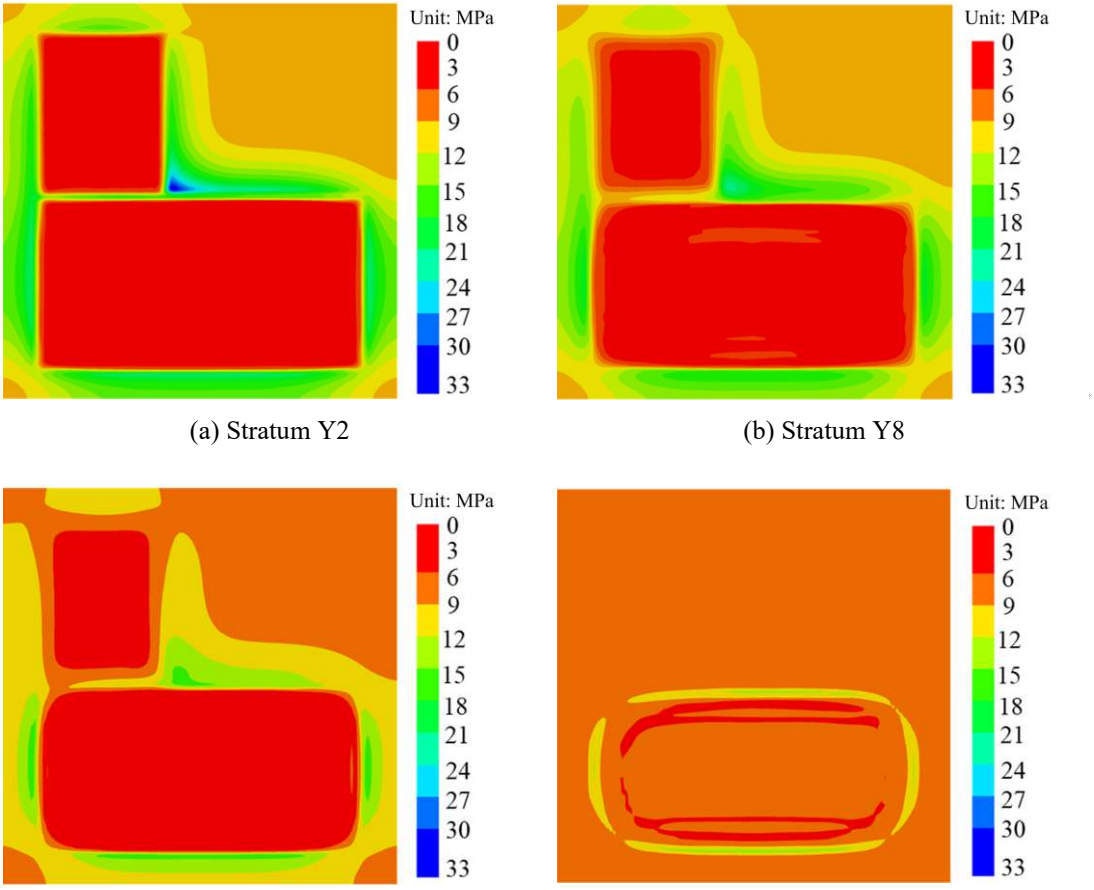
Because the coal seam dips at only 3-7 degrees and is approximately horizontal, it is simplified as a horizontal seam in the model. The seam thickness is 4.32 m, the roof strata total 99.58 m in thickness, and the floor strata total 9.1 m. Each face roadway is 6 m wide. The Mohr-Coulomb constitutive model is adopted. An overburden load of 7.15 MPa is applied at the model top, normal displacement is restrained at the bottom, and lateral stresses are set using the mine's in-situ stress measurement data.

Following the actual mining and development sequence, the model simulates extraction of I030901, development of the I030902 gob-side roadway, and extraction of I030902 in succession.

This accounts for the sequential effects of formation of the adjacent goaf and mining disturbance from the current face. Coal and rock parameters are assigned using physical and mechanical test results for the coal seam and roof and floor strata.

3.3 Stress distribution characteristics

The model results show that stress concentration positions differ among strata at different elevations in the gob-side region after I030902 advances. Y20 is included as a higher-stratum reference and is not an intended fracturing stratum. Figure 4 shows the vertical stress distributions in the different load-bearing strata.

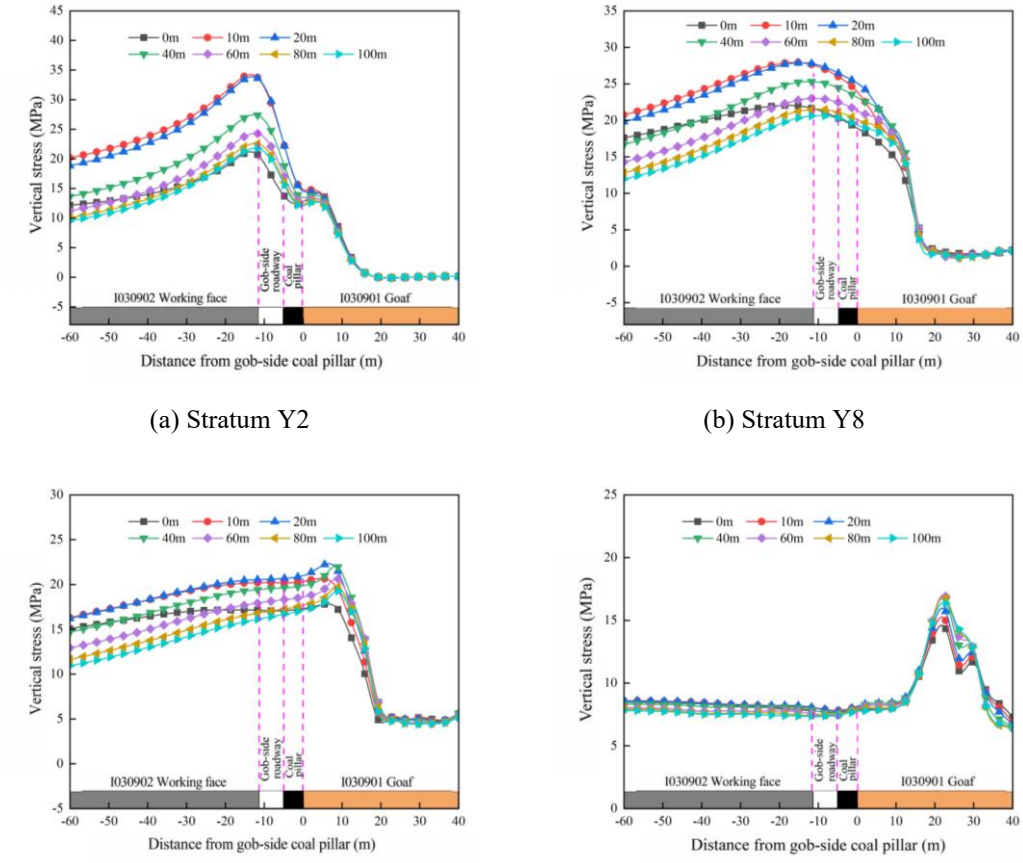


(a) Stratum Y2 (b) Stratum Y8

(c) Stratum Y13 (d) Stratum Y20

Figure 4. Vertical stress distributions in hard strata above the I030902 working face.

The contour plots show differences in the shape and location of stress concentration regions among strata. To compare lateral stress variations and peak positions, sections at the face and 10, 20, 40, 60, 80, and 100 m ahead of it are selected during I030902 extraction. Vertical stress curves are extracted along the coal seam dip direction for each stratum, as shown in Figure 5. The horizontal axis represents lateral distance from the gob-side coal pillar along the seam dip direction, and the vertical axis represents vertical stress. Legend distances indicate how far each section is ahead of the working face; 0 m denotes the section at the face.



(a) Stratum Y2

(b) Stratum Y8

(c) Stratum Y13

(d) Stratum Y20

Figure 5. Lateral vertical stress profiles in different strata ahead of the working face.

The lateral stress curves show that the vertical stress peaks in Y2 and Y8 occur mainly near the gob-side roadway, whereas the peak in Y13 shifts toward the I030901 goaf. Thus, the loading positions of the three strata do not fully coincide. Borehole design must account for treatment requirements at different elevations and lateral positions.

4. Bilateral staged hydraulic fracturing scheme and monitoring methods

4.1 Test section layout and borehole design

Previous studies show that the treatment stratum influences overburden failure and mining-induced stress responses[11]. Based on the target strata and loading characteristics identified in the preceding section, long and short boreholes are arranged on both the solid coal side and the coal pillar side of the gob-side return airway. The short boreholes target Y2, while the long boreholes target Y8 and Y13.

The test section is approximately 100 m long and lies about 500-600 m from the setup entry. S boreholes begin at 506 m and L boreholes at 500 m. Boreholes of the same type are spaced 12 m apart, with the starting positions of the two types staggered by 6 m. Each roadway side has nine S boreholes and nine L boreholes, giving 36 fracturing boreholes in total. Table 3 lists their diameters, lengths, inclinations, and staged fracturing parameters. Figure 6 shows the plan layout on both

roadway sides and their intended correspondence with the target strata. Figure 6(a) illustrates borehole spacing and the staggered long and short borehole arrangement; Figure 6(b) illustrates borehole directions and the positions of the treatment stages.

Borehole length and inclination are determined jointly by the target position and borehole collar elevation. Assuming approximately horizontal strata and straight boreholes, the geometric relationships are:

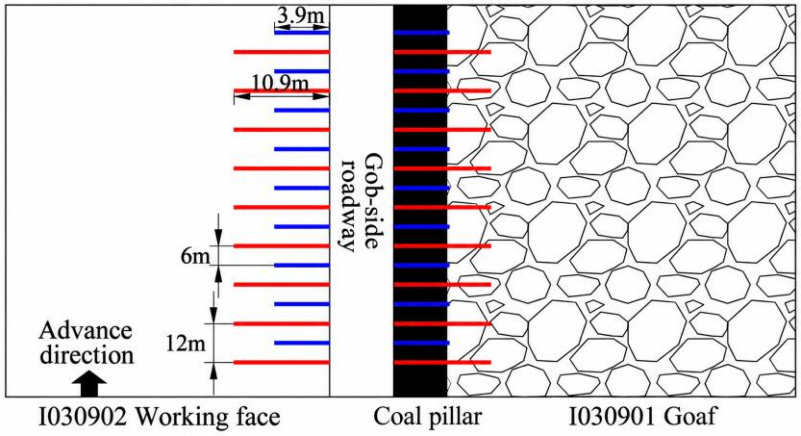
$$H - z_0 = L\sin\alpha \tag{2}$$

$$d = L\cos\alpha \tag{3}$$

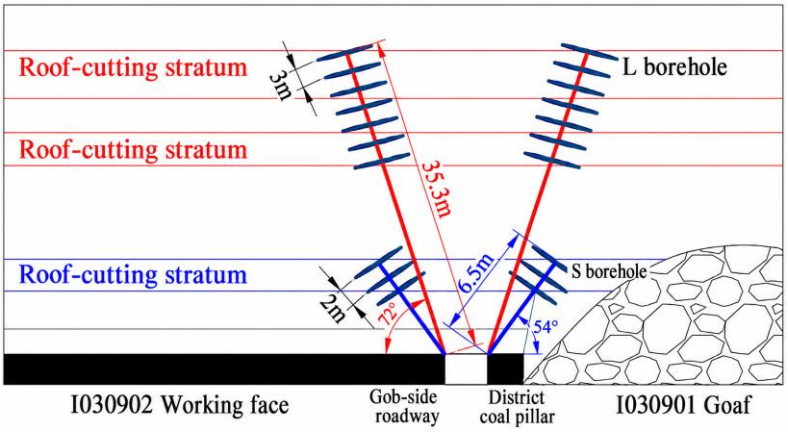
In the formula: H is the elevation of the intended treatment position relative to the coal seam roof;z_0 is the borehole collar elevation relative to the same datum;L is the borehole length;α is the angle to the horizontal plane;d is the horizontal distance.

Borehole type	Intended strata	Diameter /mm	Length /m	Inclination	Stages	Stage spacing /m
S	Y2	65	6.5	54°	3	2
L	Y8, Y13	65	35.3	72°	7	3

Table 3. Design parameters for staged fracturing in long and short boreholes.



(a) Borehole spacing and staggered long and short borehole arrangement



(b) Borehole directions and treatment stage positions

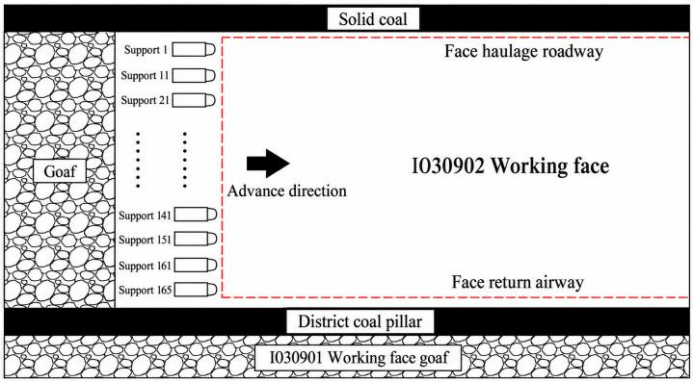
Figure 6. Bilateral long and short borehole design for staged hydraulic fracturing.

4.2 Staged fracturing procedure and field monitoring

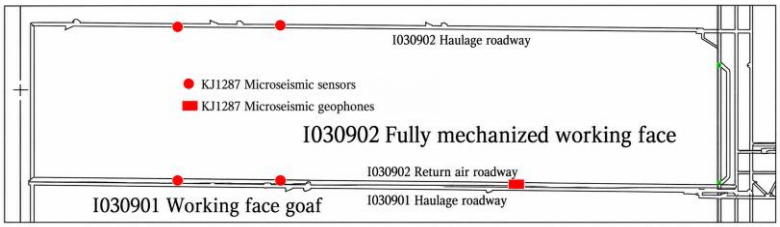
Staged hydraulic fracturing treats the rock at different positions along a borehole by isolating individual intervals and injecting water sequentially. The test uses a retreating sequence from the borehole toe toward the collar. The equipment and operating parameters are described below.

After drilling to the design depth and cleaning the borehole, a ZF-A25 double-ended inflatable packer isolates the intended treatment interval. A BZW200/31.5 high-pressure water pump injects water into the isolated interval. After treatment of that stage, the packer is withdrawn toward the collar, and the next interval is isolated and injected. This sequence continues until all stages are completed[16]. S boreholes have three stages spaced 2 m apart, and L boreholes have seven stages spaced 3 m apart. Borehole wall inspection is conducted after fracturing to observe local fracture morphology.

Previous studies have combined mining-induced stress and microseismic responses to evaluate staged roof hydraulic fracturing. To analyze surrounding rock deformation in the gob-side roadway, three monitoring stations equipped with YHW300 surrounding rock deformation instruments are installed within 100 m ahead of the I030902 face for real-time monitoring. Hydraulic support working resistance reflects ground pressure responses and serves as one indicator for evaluating roof fracturing. Support loads are monitored using the KJ24 system. Daily maximum working resistance records for supports Nos. 61, 71, 81, and 91 are selected and analyzed against face advance position to compare load changes in the unfractured and test sections. The KJ1287 system is used for microseismic monitoring, with event energy and energy levels describing coal and rock fracturing activity. Figure 7 shows the support and microseismic monitoring layouts.



(a) Hydraulic support monitoring layout



(b) Microseismic monitoring layout

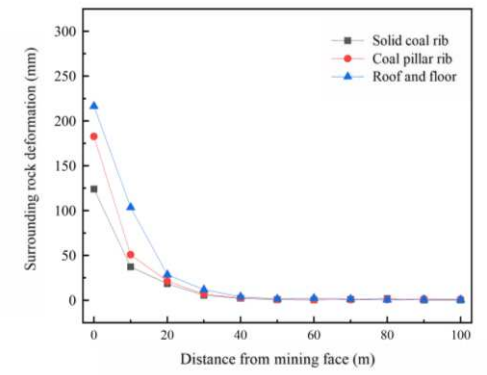
Figure 7. Hydraulic support pressure and microseismic monitoring layouts at the I030902 working face.

The unfractured support load comparison data are taken from approximately the first 200 m of extraction, whereas the test section lies 500-600 m from the setup entry.

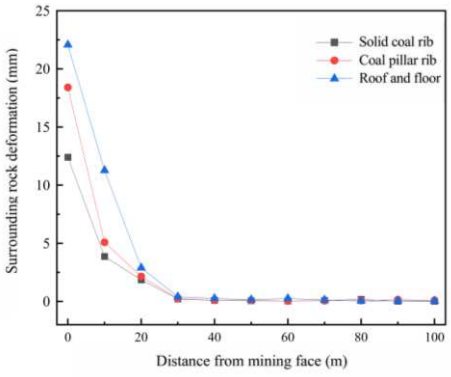
5. Field response results

5.1 Surrounding rock deformation in the gob-side roadway

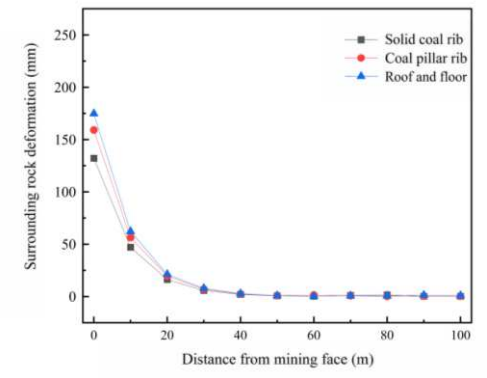
Deformation measurements from three stations in the unfractured and fractured sections are used to plot roof and floor, coal pillar rib, and solid coal rib deformation against distance from the mining face. The curves are grouped by monitoring station to compare the two sections, as shown in Figure 8.



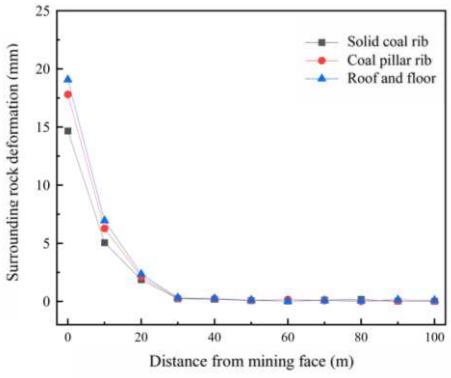
(a) Station 1 unfractured section



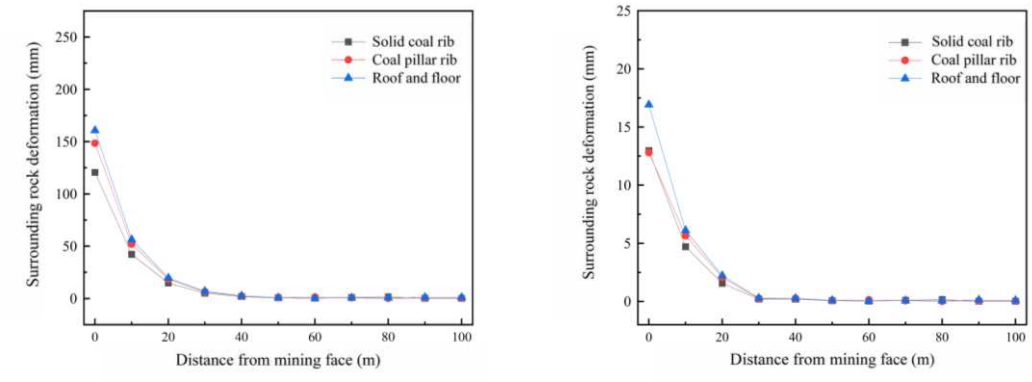
(b) Station 1 fractured section



(c) Station 2 unfractured section



(d) Station 2 fractured section



(e) Station 3 unfractured section (f) Station 3 fractured section

Figure 8. Comparison of surrounding rock deformation in unfractured and fractured sections at three monitoring stations.

In the unfractured section, the distance between the advancing face and each roadway monitoring station decreases as mining proceeds. Deformation increases progressively, with a more pronounced increase when the face approaches the station.

Among deformation directions, roof and floor deformation is larger in the unfractured section, and coal pillar rib deformation exceeds solid coal rib deformation. The difference between the two ribs becomes more pronounced near the face. Although the values differ among the three stations, all show unequal deformation of the coal pillar and solid coal ribs.

In the fractured section, deformation in each direction also increases as the station-to-face distance decreases, but its magnitude is substantially lower than in the unfractured section. Table 4 compares the reported surrounding rock deformation values for the two sections.

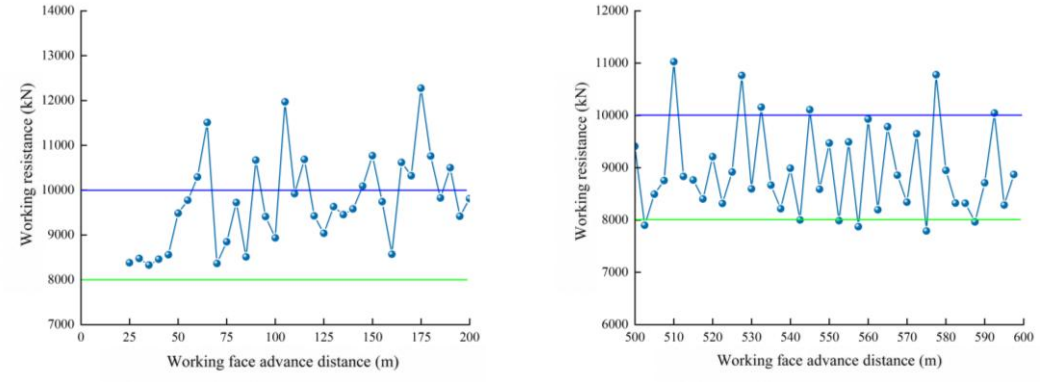
Deformation measure	Unfractured section (mm)	Test section (mm)
Roof and floor deformation	Approx. 225	Approx. 22
Coal pillar rib deformation	Approx. 180	Approx. 18
Solid coal rib deformation	Approx. 125	Approx. 12

Table 4. Reported surrounding rock deformation in unfractured and fractured sections.

The lower deformation level in the fractured section is evident in both the roof and floor direction and the two ribs.

5.2 Hydraulic support loads at the working face

Daily maximum support working resistance and daily face advance records are used to compare support loads in the unfractured and fractured sections. Figure 9 shows working resistance as a function of advance distance.



(a) Support working resistance in the unfractured section

(b) Support working resistance in the fractured section

Figure 9. Comparison of hydraulic support working resistance in unfractured and fractured sections.

Both sections show fluctuations and local peaks in working resistance, indicating variable support loading as the face advances. Mean hydraulic support working resistance decreases from 9,725 kN to 8,943 kN, a difference of 782 kN. These values correspond to an approximately 8% reduction and indicate a lower section-average load level in the fractured section.

These averages describe load levels over the two advance sections and do not imply the same reduction at every advance position. The unfractured comparison section includes the initial extraction stage, whereas the fractured section lies 500-600 m from the setup entry. Because the two datasets represent different mining stages, their mean working resistance difference must be interpreted in the context of section conditions and cannot be attributed entirely to fracturing.

5.3 Supplementary borehole wall fracture and microseismic observations

Representative post-fracturing borehole wall inspection images are selected to illustrate local fracture morphology near the fracturing boreholes. Figure 10 shows the observed fracturing result.

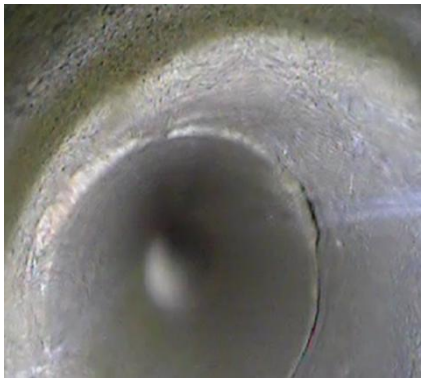
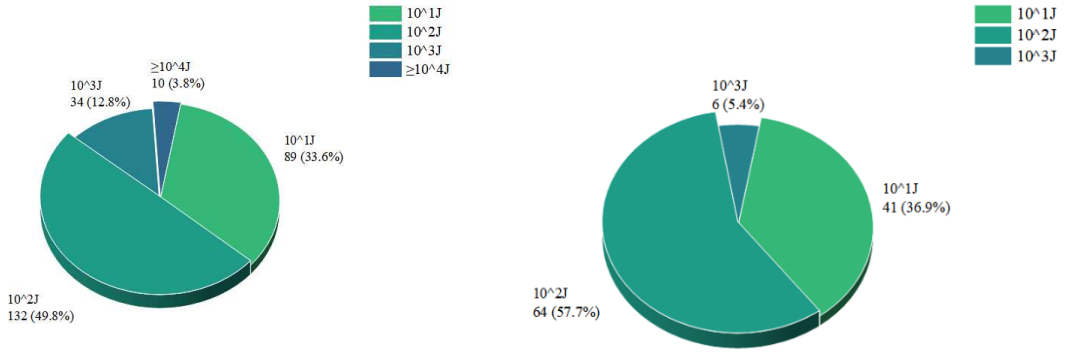


Figure 10. Borehole wall inspection after fracturing.

Existing microseismic event energy statistics are used to show event counts at different energy levels in the unfractured and fractured sections and compare their energy distributions, as shown in Figure 11.



(a) Unfractured working face section (b) Fractured working face section

Figure 11. Microseismic event energy distributions in unfractured and fractured sections.

The unfractured records contain 10 events with energies of at least 10^4 J. Records from the fractured section are dominated by events at the 10^1-10^2 J levels. The highest level shown is 10^3 J, with six events; no events at 10^4 J or above are shown. Microseismic records supplement the deformation and support load measurements with information on fracturing activity. Their interpretation is also affected by event location accuracy, and combined spatial and energy analysis helps characterize roof fracturing[27,28]. Because effective monitoring duration, advance length, and sensor coverage have not been standardized between the sections, this study compares only the energy level distributions in the available records. It does not calculate an activity reduction from total event counts or use energy statistics alone to demonstrate fracture connectivity.

Taken together, surrounding rock deformation, support loads, and microseismic records indicate that the fractured section's field response is broadly consistent with the design objectives of reducing deformation and loading. The stratified borehole arrangement provides a reference for similar gob-side roadways, while specific borehole lengths, inclinations, and spacings should be checked again against geological occurrence, target positions, and construction conditions.

6. Conclusions

(1) The overburden sequence and composite-beam load screening identify Y2, Y8, and Y13 as the intended fracturing strata. Numerical simulation indicates that stress concentrations in Y2 and Y8 lie near the gob-side roadway, whereas the Y13 stress peak shifts toward the old goaf. Differences in loading positions among strata provide a basis for stratified borehole arrangement and treatment position selection.

(2) Long and short boreholes are arranged on both sides of the gob-side roadway according to target stratum elevations and lateral loading characteristics. A staged fracturing procedure retreats from the borehole toe toward the collar. Short boreholes are intended to treat the lower Y2 stratum, while long boreholes target Y8 and Y13, addressing treatment requirements at different elevations and lateral positions. The actual correspondence between each fracturing stage and target stratum must be verified using borehole collar elevations and trajectories.

(3) Field monitoring shows lower surrounding rock deformation in the fractured section than in the unfractured section. Approximate maximum roof and floor, coal pillar rib, and solid coal rib deformation decreases from 225, 180, and 125 mm to 22, 18, and 12 mm, respectively. Mean support working resistance decreases from 9,725 kN to 8,943 kN, approximately 8%. Microseismic records

from the fractured section are dominated by events at 10^1-10^2 J, with no events at 10^4 J or above shown. These field responses are broadly consistent with the design objectives of reducing deformation and loading.

References

1. Li, Z. & Wang, R. Disaster mechanisms of thick, hard roofs and control technology using hydraulic fracturing in long directional boreholes. *Coal Science and Technology* **54**(4), 159-173 (2026).
2. Huo, B., Meng, F., Li, T. et al. Roadway protection using small coal pillars at fully mechanized top-coal caving faces in extra-thick coal seams beneath multiple hard roof strata. *Coal Science and Technology* **52**(3), 13-23 (2024).
3. Lai, X., Xu, L., Cao, J. et al. Instability characteristics and control methods for small coal pillars beside gob-side roadways under mining influence. *Coal Science and Technology* **53**(1), 39-53 (2025).
4. Kang, H., Jiang, P., Feng, Y. et al. Pressure relief technology for surrounding rock in coal mine roadways and its applications. *Coal Science and Technology* **50**(6), 1-15 (2022).
5. Wang, Q., Jiang, Z. H., Jiang, B. et al. Ground control method of using roof cutting pressure release and energy-absorbing reinforcement for roadway with extra-thick hard roof. *Rock Mechanics and Rock Engineering* **56**(10), 7197-7215 (2023).
6. Yu, B., Tai, Y., Kuang, T. et al. Theory and technical system for surface and underground control of near-field and far-field hard roofs in large-space stopes. *Journal of China Coal Society* **48**(5), 1875-1893 (2023).
7. Xu, J., Zhu, W., Xuan, D. et al. The complete-column concept of strata control and its practice. *Journal of China Coal Society* **50**(1), 166-179 (2025).
8. Xia, B. W., Zhou, Y. M., Zhang, X. G. et al. Physical and numerical investigations of target stratum selection for ground hydraulic fracturing of multiple hard roofs. *International Journal of Mining Science and Technology* **34**(5), 699-712 (2024).
9. Zhang, Y., Li, Y., Xiao, J. et al. Presplitting-induced weakening of hard overburden and the control mechanism of the water-conducting fracture zone. *Coal Science and Technology* **52**(4), 105-118 (2024).
10. Gao, X., Hao, X., Ji, J. et al. Evolution of strata structure with block size under full-stratum presplitting of high-level key strata and its effects on rockburst prevention and pressure relief. *Journal of China Coal Society* **51**(3), 1921-1933 (2026).
11. Wang, X. H., Feng, Y. J., Zhang, F. S. et al. Investigation on breakage and collapse characteristics of hard and thick roof during coal excavation subject to hydraulic fracturing. *Engineering Failure Analysis* **181**, 109935 (2025).
12. Wu, Y. Y., Liu, C. Y., Gao, Y. B. et al. Hydraulic fracturing technology for controlling surrounding rock failure under coal pillar and thick-hard roof conditions: stress-fluid-solid coupling analysis based on multi-scale DEM. *Engineering Failure Analysis* **182**, 110025 (2025).
13. Li, H., Liu, H., Liu, C. et al. Phase-field modeling and numerical simulation of pressure relief by hydraulic fractures in roadway roofs. *Journal of China University of Mining and Technology* **54**(5), 971-983 (2025).
14. Hua, X., Qi, J., Li, Z. et al. Effects of borehole angle and placement stratum on hydraulic fracturing of composite hard roofs. *Coal Science and Technology* **54**(5), 234-250 (2026).

15. Kang, H., Feng, Y., Zhang, Z. et al. Strata control technology using hydraulic fracturing in underground directional boreholes in coal mines and its applications. *Coal Science and Technology* **51**(1), 31-44 (2023).
16. Niu, T. Surrounding rock control by staged hydraulic fracturing to weaken hard stope roofs. *Coal Science and Technology* **50**(8), 50-59 (2022).
17. Hu, Q., Liu, J., Li, Q. et al. Experimental investigation of stress and fracture evolution during staged hydraulic fracturing of coal seam roofs. *Journal of China University of Mining and Technology* **52**(6), 1084-1095, 1202 (2023).
18. Zhang, Y., Ji, F., Zhao, T. et al. Combined hydraulic slotting and fracturing for roof control and pressure relief in gob-side roadways beneath hard roofs. *Journal of China Coal Society* **49**(12), 4739-4751 (2024).
19. Tan, Y., Wang, Y., He, M. et al. Multidimensional staged hydraulic fracturing for rockburst control and damage mitigation in hard roofs above deep extra-thick coal seams. *Journal of China Coal Society* **50**(2), 794-809 (2025).
20. Wang, R., Xu, G., Kang, H. et al. Surrounding rock control at a 10 m ultra-high mining-height working face in Caojiatan Coal Mine. *Journal of China Coal Society* **50**(4), 1935-1950 (2025).
21. Lei, Y., Feng, Y., Kang, H. et al. Research and application of fracturing-based pressure relief for thick, hard roofs at ultra-high mining-height working faces. *Journal of China Coal Society* **50**(4), 1907-1934 (2025).
22. Zhuang, J. X., Mu, Z. L., Cai, W. et al. Multistage hydraulic fracturing of a horizontal well for hard roof related coal burst control: Insights from numerical modelling to field application. *International Journal of Mining Science and Technology* **34**(8), 1095-1114 (2024).
23. Ma, Y., Gao, Y., Zhu, S. et al. Mechanisms and evaluation methods for rockburst prevention by surface hydraulic fracturing in coal mines. *Journal of China Coal Society* **49**(11), 4390-4405 (2024).
24. Wu, J., Xia, Y., Du, T. et al. Mine earthquake prevention and control through surface fracturing of deep multiple thick, hard roof strata. *Coal Science and Technology* **54**(5), 219-233 (2026).
25. Shuang, H., Xin, Y., Li, S. et al. Overburden fracture distribution under roof cutting and roadway retention based on key stratum theory. *Coal Science and Technology* **52**(5), 102-113 (2024).
26. He, J. H., Li, W. P., Fan, K. F. et al. A method for predicting the water-flowing fractured zone height based on an improved key stratum theory. *International Journal of Mining Science and Technology* **33**(1), 61-71 (2023).
27. Cao, A., Wang, C., Yang, X. et al. Stope fracture characterization and rockburst warning considering microseismic location accuracy. *Coal Science and Technology* **52**(2), 1-9 (2024).
28. Xu, S. D., Lei, H., Zhao, X. D. et al. Study on the failure mechanism of overlying strata under hydraulic fracturing in coal seams. *Journal of Applied Geophysics* **238**, 105725 (2025).

Acknowledgments

The authors thank all editors and reviewers for their comments and suggestions.

Author Contributions

T.L provided the original idea; Y.W wrote the main manuscript text; Y.L, Z.Z and T.W provided the data in this paper; B.L and L.N made the figures of this paper; T.L and Y.L embellished this paper; Y.W is responsible for original draft writing; Y.W is responsible for review & editing.

Competing interests

The authors declare no competing financial interest.

Funding

1. National Natural Science Foundation of China Project (Regional Science Foundation) (Grant No.5266040748);
2. Ordos Science & Technology "Breakthrough" Program – Open Competition and Top-Task Major Project (Grant No. JB20251447);
3. Ordos Flagship Innovation Team Project (Grant No. TD20240005);
4. Ordos Key Research and Development Program (Grant No. YF20250274);
5. Inner Mongolia Autonomous Region Key Research and Development and Achievement Transformation Plan Project (Social Public Welfare Field)(Grant No. 2026YFSH0189);
6. International Science and Technology Cooperation Project of Ordos High - tech Industrial Development Zone (GJKJHZ202603).